

3-dimensional simulation of long QT syndrome: early afterdepolarizations and reentry

Ray Huffaker, Boris Kogan

Abstract

Early afterdepolarizations (EADs), thought to be highly arrhythmogenic in the case of long QT (LQT) syndromes, are most readily observed at slow heart rates and suppressed by fast heart rates. However, EADs are thought to contribute to tachycardia-dependent arrhythmias such as Torsades des pointes and ventricular fibrillation, leading to sudden cardiac death. Recent studies of simulated LQT in 1D and 2D tissues have suggested a possible mechanism by which EADs could occur at rapid heart rates as a sequela of spontaneous sarcoplasmic reticulum (SR) Ca^{2+} release related to intracellular Ca^{2+} overload. These EADs could then lead to reinitiation of 1D and spiral wave reentry that otherwise would have self-terminated. This paper extends these results to simulated LQT in 3D tissue and shows that the appearance of EADs can similarly reinitiate scroll wave reentry.

Introduction

Early afterdepolarizations (EADs), thought to be highly arrhythmogenic in the case of long QT (LQT) syndromes, are most readily observed at slow heart rates and suppressed by fast heart rates ¹. However, EADs are thought to contribute to tachycardia-dependent arrhythmias such as Torsades des pointes and ventricular fibrillation, leading to sudden cardiac death. Recent studies of simulated LQT in 1D and 2D tissues have suggested a possible mechanism for this seemingly paradoxical behavior ². On the cellular level, elevated intracellular Ca^{2+} (Ca_i) during rapid pacing combines with the decreased outward membrane current due to LQT to lengthen the plateau phase of the action potential. During very rapid pacing Ca_i overload may lead to spontaneous (i.e. non voltage-gated) Ca^{2+} release from the sarcoplasmic reticulum (SR). This large influx of Ca_i could activate Ca^{2+} -sensitive inward currents, further destabilizing the plateau phase and allowing the slight reactivation of a normal Ca_L channel to trigger an EAD. On the tissue level, regions of cells undergoing simultaneous EAD were shown to reinitiate reentry in rectilinear (1D) and spiral (2D) waves that otherwise would have self-terminated. The purpose of this study is to extend these results to the conduction of scroll waves in simulated LQT in 3D tissue.

Methods

The mathematical model of wave propagation in tissue is described by the following partial differential equation:

$$\frac{\partial V}{\partial t} = D \left(\frac{\partial^2 V}{\partial x^2} + \frac{\partial^2 V}{\partial y^2} + \frac{\partial^2 V}{\partial z^2} \right) + (I_m + I_{st}(s, t)) \frac{1}{C_m} \quad (1)$$

with appropriate initial and boundary conditions.

Here V is membrane potential, D is a diffusion coefficient, I_{st} is the external stimulating current, C_m is the membrane capacitance, and x , y , and z are the space

coordinates. To make the above equation closed, it is necessary to add the system of nonlinear ordinary differential equations (ODEs) that describes the behavior of all components of I_m and processes in intracellular compartments. For this purpose we have chosen the AP model proposed by Chudin, et al. ³, which represents a modification of the Luo-Rudy AP model ⁴. The initial conditions and parameters were chosen the same as in Huffaker, et al. ².

As in Huffaker, et al. ², we simulated long QT 2 syndrome by decreasing the maximum conductivity of I_{Kr} (\bar{G}_{kr}) by 50%. As before, we also simulated a modest increase in sympathetic tone by amplifying $I_{Ca(L)}$ and $I_{p(Ca)}$, increasing the parameters $\bar{I}_{p(Ca)}$ and \bar{I}_{Ca} by 31.8%. LQT2 simulations were compared to simulations run with normal model parameters.

Computer simulations were performed on a massively parallel Opteron cluster at Lawrence Berkeley National Laboratory. The simulations used the operator splitting algorithm ⁵. According to this algorithm the integration (1) is split into two parts:

integration of diffusion equation $\frac{\partial V}{\partial t} = D \left(\frac{\partial^2 V}{\partial x^2} + \frac{\partial^2 V}{\partial y^2} + \frac{\partial^2 V}{\partial z^2} \right)$, and integration of the system of ODEs $\frac{\partial V}{\partial t} = (I_m + I_{st}) \frac{1}{C_m}$. These integrations were executed in consecutive time

cycles of predetermined duration $\Delta t = 0.1$ ms. The specific features of this algorithm are described in Chudin, et al. ⁶ and Kogan, et al. ⁷. The operator splitting algorithm allows integration of the system of nonlinear ODEs at any point in space independently and with variable time steps. In all computer simulations, the time step for ODE solutions varied from 0.005-0.1 ms and the space step Δx was fixed at 0.025 cm. These choices provided stability and accuracy with the chosen numerical integration method, and did not disturb the conditions of medium continuity ⁸. Specifically, an explicit Euler numerical method

was used to solve the diffusion equation, for which the stability condition was $\Delta t \leq \frac{\Delta x^2}{8D}$.

For $\Delta x = 0.025$ cm and $D = 1$ cm²/s, the critical value was $\Delta t \approx 0.08$ ms. In our computations this equation was solved twice in one computational cycle, with $\Delta t = 0.05$ ms. The problem of computational error arises for solutions to the system of nonlinear ODEs describing the fast membrane processes during depolarization phase of the AP. To decrease these errors, we used the Euler explicit method with variable time steps, which were changed depending on the rate of the most rapid variable. In addition, for the fast sodium channel gate variable, we replaced the Euler method with the so-called hybrid method ⁹.

The continuity condition proposed by Winfree ⁸ requires that the chosen space step Δx satisfies the inequality $D > \Delta x^2 / T_r$. Here T_r is an activation rising time measured in a cell placed in tissue. This time is longer than in an isolated cell due to the effect of the local currents and incomplete recovery of I_{Na} during wave circulation in a comparatively short ring length. Estimating $T_r = 2.5$ ms, we found that for $D = 1$ cm²/s and $\Delta x = 0.025$ cm, this inequality was well satisfied.

The tissue was simulated as a right square prism grid of 256 x 256 x 30 diffusively-coupled nodes ($D = 1$ cm²/s) with no-flux boundary conditions. The space

step $\Delta x = 0.025$ cm yields a tissue size of $6.4 \times 6.4 \times 0.75$ cm². This tissue size is very large compared to most physiological values, but allows us to avoid the effects of the border conditions. Individual nodes were distinguished by their position in the grid with an ordered pair (x, y, z) . The upper left node of the front face was denoted as $(0,0,0)$ and the lower right node of the rear face denoted as $(255,255,29)$. The parallel processors were distributed over the entire grid in stripes, so each processor integrates only in its own part of the grid. The communication between processors was implemented using Message-Passing Interface. The velocity of a rectilinear front propagation was approximately 55 cm/s.

Results

The results of 3D simulation are visualized as 2D cross sections (Fig. 1) and the outer surface (Fig. 2) of the 3D tissue.

First, a stimulus current was applied to nodes $\{(x,y) \mid y \leq 20\}$ in the top layer ($z = 0$) of the tissue (Fig. 1A, $t = 0.005$ s). This produced a rectilinear wave traveling from left to right across the tissue. A premature stimulus was then applied near the tail of the spiral wave (Fig. 1 and Fig. 2A, $t = 0.275$ s), inducing a scroll wave rotating in the clockwise direction ($t = 0.825$ s).

The premature stimulus was applied to all layers ($0 \leq z \leq 30$). If only applied in the top layer, the premature stimulus would need to propagate downward to stimulate the bottom layer. By the time it reached the bottom layer, the rectilinear wave would have propagated further to the right and the premature stimulus would be too far from the tail of the wave, causing a circular wave rather than a scroll wave.

In the case of normal cardiac cell model parameters, stationary scroll wave conduction became nonstationary after a few seconds of simulation, due to accumulation of Ca_i and I_{spon} . The nonstationary scroll wave reentry was then sustained. In the LQT2 case, nonstationary conduction eventually led to a stop of propagation (Fig.1 and Fig. 2A, $t = 2.450$ s). As described in Hufaker, et al. ², increasing Ca_i accumulation prolonged the baseline APD. The mismatch between the resultant longer wavelength and fixed tissue size led to conduction block. Rather than terminating reentry, however, the Ca^{2+} subsystem irregularity, in particular I_{spon} , led to the development of EAD (Fig. 2C) and reinitiation of reentry (Fig. 1 and Fig. 2A, $t = 2.585$ s) once a region of repolarized tissue appeared. A new scroll wave formed in the same clockwise direction as the wavefront followed the path of inhomogeneous repolarization (Fig. 1 and Fig. 2A, $t = 2.650$ s).

The importance of I_{spon} in reinitiating the scroll wave is illustrated in Fig. 2B. When I_{spon} was disabled in the cell model at the time propagation stopped ($t = 2.450$ s), reentry was terminated when the spiral wave meandered off the tissue. EADs were less prominent (Fig. 2C) and incapable of causing wave regeneration. The entire tissue entered repolarization phase (Fig. 2B, $t = 2.585$ s) and eventually returned to rest potential. Thus, I_{spon} is a necessary factor for the appearance of strong EADs and subsequent reinitiation of reentry.

A close look at Fig. 1 shows virtually identical wave conduction among the different cross-sections of the 3D tissue. This is because the size of the z -dimension is relatively small (30 nodes) compared to the x - and y -dimensions (256 nodes), but the rate of diffusion in all three dimensions is equal. This leads to synchronization of the layers

of the tissue. Future work introducing inhomogeneity in the cells of different layers of the tissue (epi-, m-, and endo-cardial cells) may cause variations in conduction among the different layers.

Discussion

The findings presented here further illuminate the potential proarrhythmic behavior of the Ca^{2+} subsystem in the pathogenic myocardium. Previous simulations² showed that the appearance of EADs at rapid heart rates, under the conditions of long QT syndrome and increased sympathetic stimulation, could reinitiate reentry of otherwise terminating 1D rectilinear waves and 2D spiral waves. The mechanism behind EAD formation was discovered to be accumulation of Ca_i leading to Ca_i overload and spontaneous Ca^{2+} release. Increased Ca_i and decreased K^+ current due to long QT syndrome prolong the APD and make the balance of repolarization currents more tenuous. Spontaneous Ca^{2+} release further increases Ca_i , strengthening Ca^{2+} -mediated inward currents and causing the already vulnerable balance of currents to swing to a prevailing inward current.

The simulation study performed here shows that this same mechanism is capable of reinitiating reentry of a scroll wave in 3D tissue. Extension of the mechanism to 3D is appealing from a physiological and clinical standpoint, as the real heart is 3D. However, the simulations were performed on homogenous isotropic tissue, whereas the real heart contains pre-existing electrophysiological and anatomic heterogeneities. Although in the real heart there may be differential regional sensitivities to spontaneous SR Ca^{2+} release and EADs, this is not likely to affect our basic conclusions. In addition, nonuniform anisotropy and transmural action potential gradients may promote drift of scroll waves towards tissue borders, perhaps amplifying both the likelihood of termination and regeneration by the mechanism we have proposed.

Conclusions

The mechanism of spiral wave regeneration by Ca_i -induced EADs could be clinically important in prolonging the duration of reentry initially triggered by EADs, thereby enhancing the risk of VF and sudden cardiac death in patients with congenital or acquired LQT syndromes. Although as yet there is no direct experimental evidence to support this hypothesis in real hearts, this simulation study provides an incentive to look for this mechanism in the experimental setting. The regeneration of the spiral wave in the original or opposite direction¹⁰ might be the most recognizable indication, although the 3D nature of real cardiac tissue may make the experimental mapping data difficult to interpret unequivocally. Intermittent reversal of spiral wave might contribute to the variable electrical QRS axis characteristic of Torsades de pointes. Our simulation conditions may not be that far off from clinically relevant ones, since spiral waves which drift without breaking up have been documented experimentally¹¹, and acquired and congenital long QT syndromes are characterized by many nonsustained episodes of unstable VT which self-terminate. This implies that the prolonged wavelength from APD lengthening is at the edge of sustainable reentry, similar to the conditions under which spiral wave regeneration was observed here. However, the relevance of this mechanism

of spiral wave regeneration to the real heart will have to await simulation on realistic 3D geometries and experimental confirmation.

Our findings may also be relevant to failed defibrillation shocks, in which post-shock EADs due to spontaneous SR Ca^{2+} release might reinitiate reentry.

Acknowledgments

The study was supported in part by NIH/NHLBI SCOR in Sudden Cardiac Death P50 HL52319. Supercomputing resources were provided by the National Energy Research Scientific Computing Center, Office of Energy Research of the US Department of Energy, under the contract #DEAC0376SF00098.

References

1. Peters NF, Cabo C, Wit AL. Arrhythmogenic mechanisms: automaticity, triggered activity and reentry. In: Zipes DP, Jalife J, eds. *Cardiac electrophysiology: from cell to bedside*. 3 ed. Philadelphia: W.B.Saunders Company; 2000:348-349.
2. Huffaker R, Lamp ST, Weiss JN, Kogan B. Intracellular calcium cycling, early afterdepolarizations, and reentry in simulated long QT syndrome. *Heart Rhythm*. 2004; 4:441-448.
3. Chudin E, Goldhaber J, Garfinkel A, Weiss J, Kogan B. Intracellular Ca^{2+} dynamics and the stability of ventricular tachycardia. *Biophys J*. 1999;77(6):2930-2941.
4. Luo CH, Rudy Y. A dynamic model of the cardiac ventricular action potential .1. Simulations of ionic currents and concentration changes. *Circ. Res*. 1994;74:1071-1096.
5. Strang G. Numerical Analysis. *SIAM. J*. 1969; 5:526-517.
6. Chudin E, Garfinkel A, Weiss J, Karplus W, Kogan B. Wave propagation in cardiac tissue and effects of intracellular calcium dynamics (computer simulation study). *Prog Biophys Mol Biol*. 1998;69(2-3):225-236.
7. Kogan BY, Karplus WJ, Chudin EE. Heart fibrillation and parallel supercomputers. Paper presented at: Proceedings of International Conference on Information and Control, 1997; St. Petersburg, Russia.
8. Winfree AT. Heart muscle as a reaction-diffusion medium: the roles of electrical potential diffusion, activation front curvature, and anisotropy. *Int.J.Bif.& Chaos*. 1997;7(3):487-526.
9. Chudin E. *Instability of Cardiac Excitation Wave Propagation and Intracellular Calcium Dynamic* [PhD]. Los Angeles: Biomathematics, University of California, Los Angeles; 1999.
10. Kogan B, Lamp, S., Weiss, J. Role of Intracellular Ca^{2+} Dynamics in Supporting Spiral Wave Propagation. In: Bekeg G, Kogan B, eds. *Modeling and Simulation*. Boston/London/Dordrecht: Kluwer Academic Publishers; 2003:177-193.
11. Davidenko JM, Pertsov AV, Salomonsz JR, Baxter W, Jalife J. Stationary and drifting spiral waves of excitation in isolated cardiac muscle. *Nature*. 1992;355:349-351.

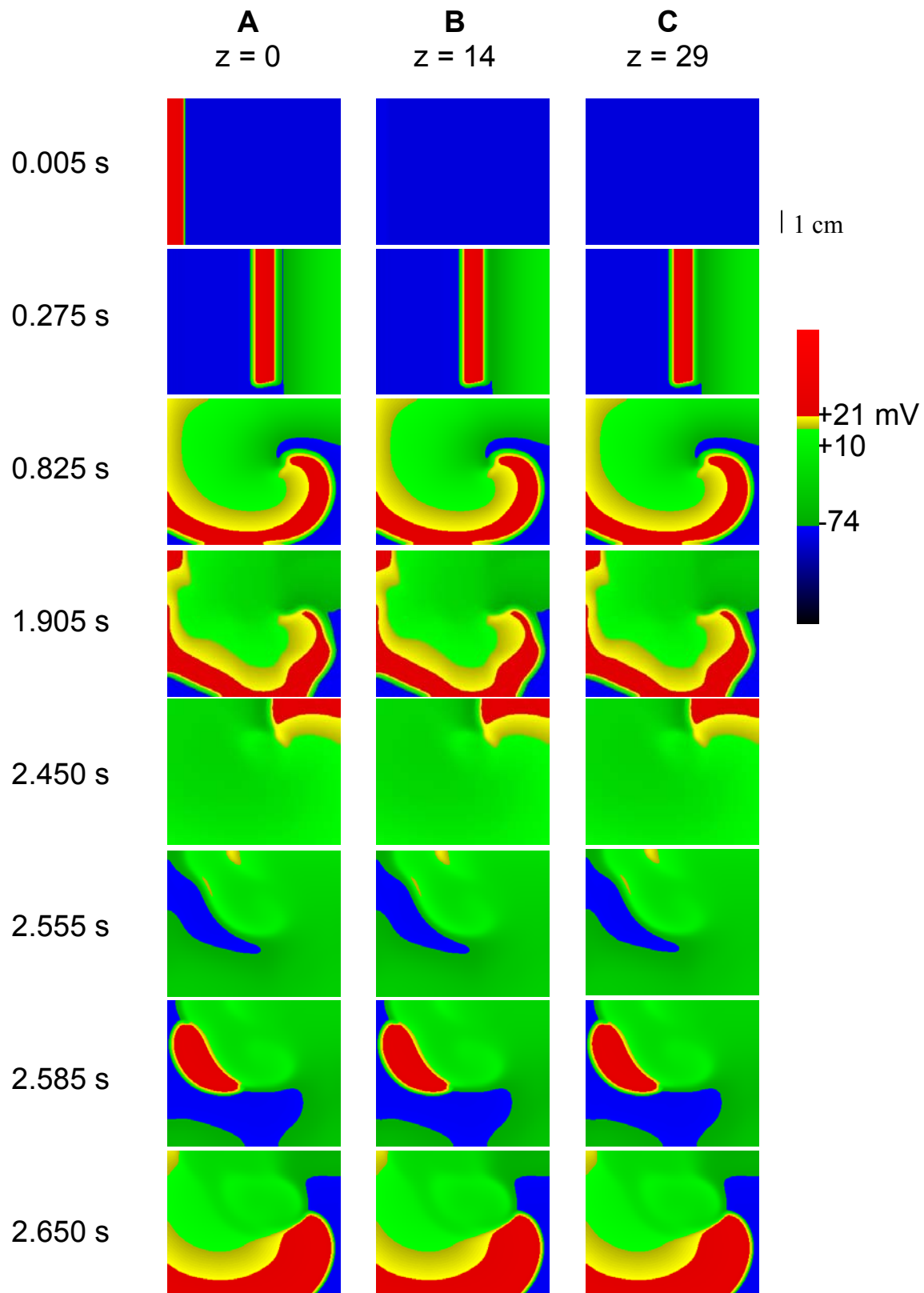


Fig 1. 3D propagation – a view of 2D cross sections

Simulated LQT2, 256 x 256 x 30 node tissue (6.4 cm x 6.4 cm x 0.75 cm)

A: top layer of tissue ($z = 0$)

B: middle layer of tissue ($z = 14$)

C: bottom layer of tissue ($z = 29$)

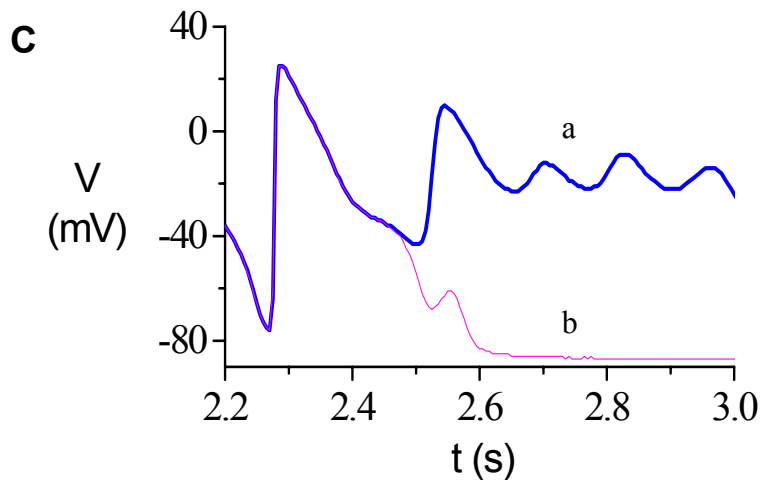
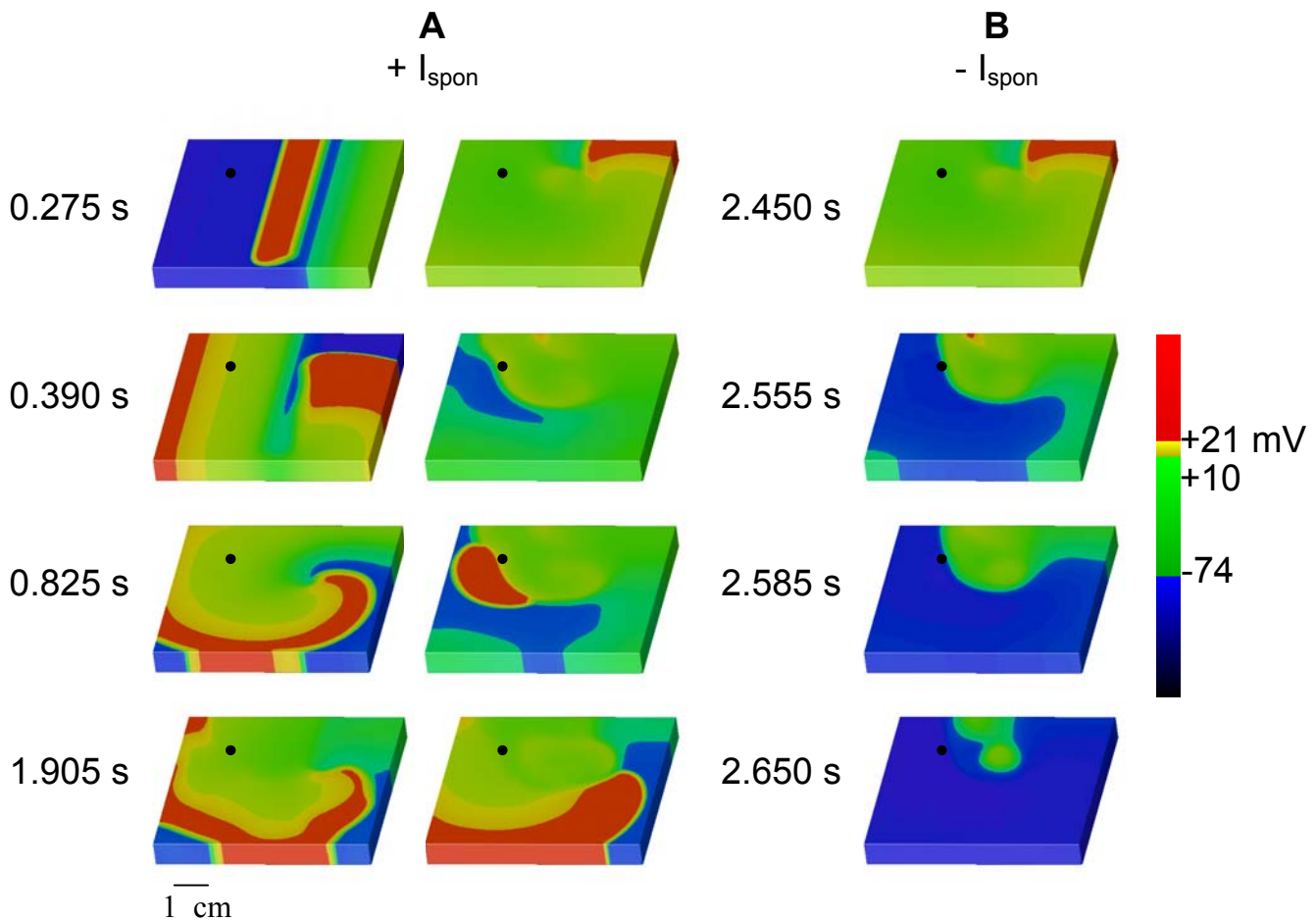


Fig 2. Effect of spontaneous Ca^{2+} release on 3D propagation with decreased \mathbf{G}_{kr}
 Simulated LQT2, 256 x 256 x 30 node tissue (6.4 cm x 6.4 cm x 0.75 cm)
 A: I_{spon} enabled
 B: I_{spon} disabled at time $t = 2.450$ s
 C: V in node (68,72,0), represented by the black dot in 1A and 1B, for the case with I_{spon} enabled (a) and I_{spon} disabled at time $t = 2.450$ s (b)